JOURNAL OF AIRCRAFT
Vol. 41, No. 3, May–June 2004

Application of Active-Aeroelastic-Wing Technology to a Joined-Wing Sensorcraft

Gregory W. Reich*
U.S. Air Force Research Laboratory, Wright-Patterson Air Force Base, Ohio 45433
and
Daniella E. Raveh† and P. Scott Zink‡
Georgia Institute of Technology Atlanta, Georgia 30332

A study was conducted to investigate the applicability of active-aeroelastic-wing technology to a joined-wing sensorcraft configuration for the purpose of minimization of embedded antenna deformations. The study was performed using a half-span aeroelastic model of a joined-wing sensorcraft design with six control surfaces. These control surfaces were used concurrently to minimize the elastic deformations at structural nodes corresponding to the antenna tip, while trimming the aircraft to a required 1-*g* level flight, simultaneously satisfying constraints on the allowable hinge moments and maximum control surface deflections. Comparison of antenna displacements for the optimized and baseline cases (using one control surface at a time) demonstrates that the active-aeroelastic-wing concept can be used to significantly reduce the antenna displacements, potentially improving the performance of the embedded antenna system. Aeroelastic displacements from the trim-optimized system are an order-of-magnitude smaller than those of the baseline. These results demonstrate the feasibility of active-aeroelastic-wing technology for the improvement of embedded antenna performance caused by structural deformations.

Nomenclature

AICS	=	aerodynamic influence coefficient matrix
D	=	relates flexible and rigid-body displacements
dv	=	design variable
e	=	design variable for nonlinear optimization
F_A	=	aerodynamic force vector
HM	=	hinge moment
K	=	stiffness matrix
LHSA, *RHSA*	=	left- and right-hand side of trim equation
M	=	mass matrix
m_r	=	rigid-body mass matrix
PA	=	aerodynamic trim forces
q	=	dynamic pressure
R	=	elements of the trim equation
u	=	displacements
wz	=	vertical displacements at finite element nodes
*wz*0	=	reference displacements at finite element nodes
α	=	angle of attack
δ	=	trim parameter
ϕ_R	=	rigid-body mode matrix

Subscripts

i, *j*	=	individual element of a vector or column of a matrix
l	=	"left-over" partition of the displacement set (as opposed to the rigid-body partition)
r	=	rigid-body partition of the displacement set
n	=	nodal index

Presented as Paper 2002-1633 at the 43rd Structures, Structural Dynamics, and Materials Conference, Denver, CO, 21 April 2002; received 15 October 2002; revision received 12 May 2003; accepted for publication 8 September 2003.

*Research Aerospace Engineer, Air Vehicles Directorate, AFRL/VASA, 2210 Eighth St., Room 219. Senior Member AIAA.

†Research Engineer II; currently Senior Lecturer, Faculty of Aerospace Engineering, Technion—Israel Institute of Technology, Haifa 32000, Israel. Member AIAA.

‡Graduate Research Assistant; currently Senior Aeronautical Engineer, Lockheed Martin Aeronautics Company, P.O. Box 748, Fort Worth, TX 76101. Member AIAA.

Trim-Optimization Problem

THE active-aeroelastic-wing (AAW) concept makes use of multiple control surfaces to reshape the wing in order to obtain some objective, while trimming the aircraft to a prescribed maneuver. The process in which the deflections of the various control surfaces are determined is referred to as trim optimization. In the general case, the trim optimization problem is one in which multiple control surfaces are used to minimize an objective function, subject to component load constraints, control surface deflection limits, and trim balance requirements for a user-defined maneuver. Various trim-optimization objectives, described in the literature, include those related to aerodynamic performance [e.g., drag minimization or maximization of lift-to-drag ratio (L/D)] or structural performance (e.g., minimization of root bending moment for symmetric maneuvers or hinge moments for antisymmetric maneuvers). Details on various trim-optimization objectives can be found elsewhere.[1–7]

At its most fundamental level, the use of multiple control surfaces represents a change in the wing's shape: specifically, a change in the camber distribution or wing twist across the span. By changing control surface settings at different trim conditions, one is in effect shaping the wing for each design point. Recent activities at the U.S. Air Force Research Laboratory,[8] NASA,[9] and DARPA[10] in the area of morphing aircraft are taking this idea to the extreme. Morphing aircraft programs hope to explore the ability to make major shape changes to an aircraft's wing for the purposes of enabling vastly different mission capabilities with the same vehicle platform. AAW is considered the pioneering first step in this direction.

For the joined-wing sensorcraft configuration, load alleviation via AAW technology can be highly valuable as the fuel load may constitute as much as 60% of the takeoff gross weight of the vehicle. In such a case, fuel consumption throughout the flight results in a change of the inertial loading, which in turn changes the shape of the elastic wing, and provides less inertial relief for section loads. The ability to consistently reduce structural loads then has the potential to reduce vehicle weight, always a major concern for the designer. Additionally, aerodynamic performance objectives for optimum L/D,

minimum drag, etc., might also be addressed in the framework of the trim-optimization problem.

Instead, in the current study the trim-optimization objective for the joined-wing sensorcraft is determined from performance considerations of the antenna that is embedded in the diamond-shaped structure. A critical issue in the performance of the antenna at high frequencies is the ability to shape the beam properly when the antenna itself is no longer flat. That is, the antenna performance is degraded under wing deformation. There are two possible solutions to the problem. One is to feed back antenna deformations to the antenna control software for compensation during beam forming (phase shifting). This approach is successful at uhf frequencies for deformations on the order of feet. As the antenna operating frequency increases, the maximum allowable deformation is reduced. At X-band, the limit is on the order of an inch. As antenna technology increases to even higher frequencies, this limit will go down even further. The second approach to the problem is to minimize the antenna deformations in the first place. Realistically, some combination of these two solutions can be adopted.

A flat antenna position in the nominal cruise condition might be achieved through a jig-shape design. The unloaded structure of the wing could potentially be designed such that at a specific point in the flight profile, with a specific load distribution, the wing assumes a flat shape in the antenna regions. However, once the load condition changes the elastic deformations will change, and the antenna will no longer be flat. Such a situation might be a result of a variation in altitude, or a change of the inertial loads caused by fuel consumption. With a proper scheduling of the control surface deflections, the elastic deformations in the antenna regions could be minimized for any given loading condition. Therefore, the trim-optimization objective for this task was set as the minimization of the structural elastic deformations at structural nodes corresponding to the outboard end of the phased-array antenna. Constraints included satisfaction of the trim condition, hinge-moment limits, and maximum and minimum allowable deflection of the control surfaces. Minimization of the objective was obtained by the trim-optimization procedure described in the following section.

Mathematical Formulation of the Trim-Optimization Problem

The formulation of the static aeroelastic equations follows the formulation provided in the ASTROS Theoretical Manual.[11] It is repeated here in order to provide the basis for the sensitivity formulation that follows.

The static equilibrium equation in physical discrete coordinates is

$$\begin{bmatrix} K_{ll} & K_{lr} \\ K_{rl} & K_{rr} \end{bmatrix} \begin{Bmatrix} u_l \\ u_r \end{Bmatrix} + \begin{bmatrix} M_{ll} & M_{lr} \\ M_{rl} & M_{rr} \end{bmatrix} \begin{Bmatrix} \ddot{u}_l \\ \ddot{u}_r \end{Bmatrix} = \begin{Bmatrix} F_{A_l} \\ F_{A_r} \end{Bmatrix} \tag{1}$$

For an unrestrained aircraft, Eq. (1) is solved together with Eq. (2), which states the requirement that the structural displacements of the free aircraft be orthogonal to the rigid-body modes with respect to the mass matrix:

$$[\phi_R]^T [M]\{u\} = \{0\} \tag{2}$$

where the rigid-body mode matrix is defined as

$$[\phi_R] = \begin{bmatrix} D \\ I \end{bmatrix} = \begin{bmatrix} -K_{ll}^{-1} K_{lr} \\ I \end{bmatrix} \tag{3}$$

and each column of $[D]$ represents the rigid-body displacements at the l-set degree of freedom (DOF) as a result of a unit displacement in one of the r-set DOF.

Substituting Eq. (3) into the orthogonality condition of Eq. (2) and merging it with the aeroelastic Eq. (1), while neglecting the elastic accelerations, results in the full set of trim equations:

$$\begin{bmatrix} K_{ll} & K_{lr} & M_{ll}D + M_{lr} \\ K_{rl} & K_{rr} & M_{rl}D + M_{rr} \\ D^T M_{ll} + M_{rl} & D^T M_{lr} + M_{rr} & 0 \end{bmatrix} \begin{Bmatrix} u_l \\ u_r \\ \ddot{u}_r \end{Bmatrix} = \begin{Bmatrix} F_{A_l} \\ F_{A_r} \\ 0 \end{Bmatrix} \tag{4}$$

The linear aerodynamic forces, translated to the structural DOF, are given by

$$\{F_A\} = q[AICS]\{u\} + [PA]\{\delta\} \tag{5}$$

Substituting Eq. (5) into Eq. (4) and rearranging terms yields:

$$\begin{bmatrix} KA_{ll} & KA_{lr} & M_{ll}D + M_{lr} \\ KA_{rl} & KA_{rr} & M_{rl}D + M_{rr} \\ D^T M_{ll} + M_{rl} & D^T M_{lr} + M_{rr} & 0 \end{bmatrix} \begin{Bmatrix} u_l \\ u_r \\ \ddot{u}_r \end{Bmatrix} = \begin{bmatrix} PA_l \\ PA_r \\ 0 \end{bmatrix} \{\delta\} \tag{6}$$

where

$$[KA] = [K] - q[AICS] \tag{7}$$

Following the procedure for solving Eq. (6) outlined in Ref. 11, the first row of Eq. (6) is multiplied by D^T and added to the second row. This new second row is interchanged with the third row to give

$$\begin{bmatrix} KA_{ll} & KA_{lr} & M_{ll}D + M_{lr} \\ D^T M_{ll} + M_{rl} & D^T M_{lr} + M_{rr} & 0 \\ D^T KA_{ll} + KA_{rl} & D^T KA_{lr} + KA_{rr} & m_r \end{bmatrix} \begin{Bmatrix} u_l \\ u_r \\ \ddot{u}_r \end{Bmatrix} = \begin{bmatrix} PA_l \\ 0 \\ D^T PA_l + PA_r \end{bmatrix} \{\delta\} \tag{8}$$

where

$$m_r = D^T M_{ll} D + D^T M_{lr} + M_{rl} D + M_{rr} \tag{9}$$

is the rigid-body mass matrix. For compact notation, Eq. (8) is rewritten as

$$\begin{bmatrix} R_{11} & R_{12} & R_{13} \\ R_{21} & R_{22} & 0 \\ R_{31} & R_{32} & R_{33} \end{bmatrix} \begin{Bmatrix} u_l \\ u_r \\ \ddot{u}_r \end{Bmatrix} = \begin{bmatrix} PA_l \\ 0 \\ D^T PA_l + PA_r \end{bmatrix} \{\delta\} \tag{10}$$

The l-set displacement vector $\{u_l\}$ is extracted from the first row of Eq. (10) and substituted into the second and third rows, resulting in

$$\begin{bmatrix} K_{11} & K_{12} \\ K_{21} & K_{22} \end{bmatrix} \begin{Bmatrix} u_r \\ \ddot{u}_r \end{Bmatrix} = \begin{bmatrix} P_1 \\ P_2 \end{bmatrix} \{\delta\} \tag{11}$$

where

$$[K_{11}] = R_{22} - R_{21} R_{11}^{-1} R_{12} \tag{12a}$$

$$[K_{12}] = -R_{21} R_{11}^{-1} R_{13} \tag{12b}$$

$$[K_{21}] = R_{32} - R_{31} R_{11}^{-1} R_{12} \tag{12c}$$

$$[K_{22}] = R_{33} - R_{31} R_{11}^{-1} R_{13} \tag{12d}$$

$$[P_1] = -R_{21} R_{11}^{-1} PA_l \tag{12e}$$

$$[P_2] = -R_{31} R_{11}^{-1} PA_l + D^T PA_l + PA_r \tag{12f}$$

The first row of Eq. (11) can be solved for $\{u_r\}$:

$$[K_{11}]\{u_r\} = [P_1]\{\delta\} - [K_{12}]\{\ddot{u}_r\} \tag{13}$$

Substituting $\{u_r\}$ of Eq. (13) into the second row of Eq. (11) yields the basic equation for static aeroelastic analysis:

$$\left[K_{22} - K_{21}K_{11}^{-1}K_{12}\right]\{\ddot{u}_r\} = \left[P_2 - K_{21}K_{11}^{-1}P_1\right]\{\delta\} \tag{14}$$

which can be written in a shortened notation as

$$[LHSA]\{\ddot{u}_r\} = [RHSA]\{\delta\} \tag{15}$$

For trimmed maneuvers, which are defined by their rigid-body accelerations $\{\ddot{u}_r\}$, Eq. (15) is solved for the free trim parameters of $\{\delta\}$.

For the AAW case, in which the number of unknown trim parameters is larger than the number of rigid-body accelerations, Eq. (15) cannot be explicitly solved for the trim parameters. These unknown trim parameters are determined via optimization, based on a user-defined objective. The trim equation, Eq. (15), serves as an optimization constraint together with other possible aeroelastic constraints. The following section describes the sensorcraft model, as well as the formulation of the trim-optimization problem specifically for the sensorcraft, with its unique objective and constraints.

Trim Optimization and the Sensorcraft Model

The sensorcraft model used here was the result of a technology assessment study,[12] which was used to identify current and future technologies required for a sensorcraft vehicle to perform the unmanned aerial vehicle (UAV) intelligence, surveillance and reconnaissance (ISR) mission. This mission has a 3000-n mile radius combined with a 40-h loiter period, which represents a 150% increase in mission radius and 67% increase in time on station compared to the Global Hawk.[13] To focus the benefits of certain technologies on the mission effectiveness, a vehicle conceptual design was created that met all of the UAV ISR requirements, as well as sensor requirements provided by the sensors community. The design, shown in Fig. 1, represented a significant departure from traditional aircraft design philosophy. In this case, the air vehicle was designed around the antennas, and all of the performance requirements were driven by antenna requirements.

One of the most important requirements for the vehicle to meet was 360-deg radar coverage. Of the few possible configurations that met this requirement, a joined-wing design with dual, offset fuselages was selected. Both vhf (a long wire) and X-band (flat phased-array panels) antennas were to be carried, as shown in Fig. 1. The phased arrays were mounted on the front face of the wing structural box on the forward wings and on the rear face of the wing box on the rear wings. The motivation for this study is the deformation of the X-band panels that are attached to the wing box. The vhf antenna operates at a sufficiently low frequency to be unaffected by deformations. However, the deformation of the X-band antenna is potentially great enough to significantly reduce its performance.

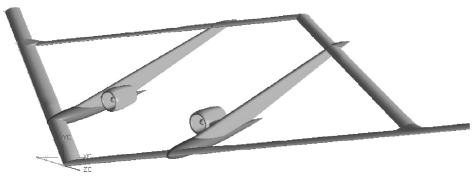

Fig. 1a Artist's rendition.

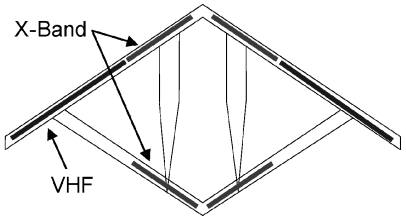

Fig. 1b Antenna placement.

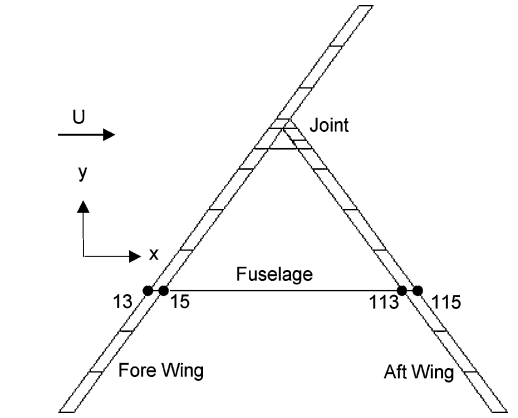

a) Top view

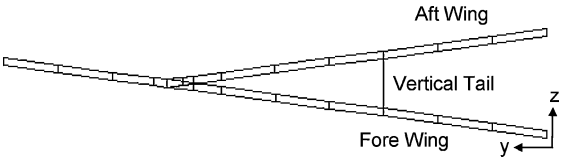

b) Front view

Fig. 2 Sensorcraft finite element model.

Finite Element Model

The finite element model, shown in Fig. 2, is a half-span model of the dual-fuselage, joined-wing sensorcraft vehicle. The fore and aft wing boxes include skins (membrane elements), spars and ribs (shear elements), and stringers (rod elements). The off-center fuselage is represented by beam elements with large cross-sectional properties, and the vertical tail, connecting the rear fuselage to the aft wing, is modeled with beam elements representing a main spar. The structural model is sized for strength, buckling, and flutter, and represents minimum gauge thickness of the ribs, spars, and skins over most of the structure. Only the skins and spars of both wings from the root out to the fuselage have larger than minimum gauge thickness. Stiffening the wing to limit deformation was not considered, as any increase in root wing stiffness would also increase vehicle weight and limit the vehicle performance, possibly to the degree that it would no longer meet the baseline mission requirements.

The antennas are modeled as nonstructural masses along the fore and aft wings themselves, as the antennas are not assumed to contribute significant stiffness to the spars on which they are mounted. Nonstructural masses are also included for avionics and sensor electronics, landing gear, engines, and fuel. The physical placement of these items is based on stability and control c.g. calculations made by the technology assessment team. Symmetric boundary conditions are applied to centerline nodes by setting the displacements of the antisymmetric degrees of freedom (that is, the y displacement and the rotations about the x and z axes) to zero. The structural nodes at which the trim-optimization objective function is applied are also indicated in the figure.

Aerodynamic Model

The aerodynamic panel model for the sensorcraft is shown in Fig. 3. It consists of six aerodynamic surfaces: the fore wing, the outer fore wing, the aft wing, the joint, the vertical tail, and the cylindrical fuselage. The baseline design resulting from the technology assessment process identified three control surface locations: a pitch flap at the trailing edge of the fore wing inboard of the fuselage, an outboard aileron/trailing-edge flap outboard of the joint, and a spoiler/deflector on the aft wing outboard of the fuselage, used as a yaw control device. For the purposes of this study, six control surfaces are created, some of which coincide with the original control surface locations. Because of the potential interference with the antennas, control surfaces are limited to the leading edge on the rear

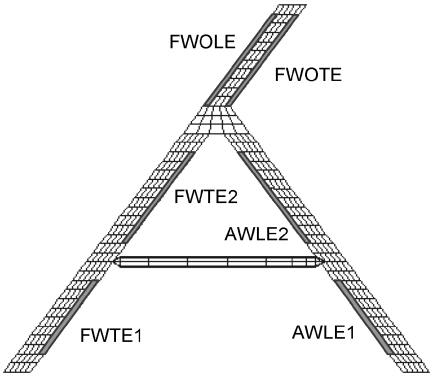

Fig. 3 Sensorcraft aerodynamic model.

wings and the trailing edge on the forward wings. These control surfaces, indicated in the figure, each cover 20% of the chord.

Trim Optimization Applied to the Sensorcraft Model

The joined-wing sensorcraft trim-optimization problem is defined as the minimization of the elastic deformations of a chosen set of structural DOF, subject to hinge-moment constraints, control surface deflection limits, and trim balance requirements for the chosen set of design points (in this case, a 1-g cruise condition). Because the objective and constraints can be expressed as a linear function of the design variables (as a result of the use of linear structural and aerodynamic models), the trim-optimization problem is posed as a linear-programming (LP) problem and solved by the simplex method.[14]

The trim-optimization problem is posed as follows:

Minimize:

$$f = \sum_{i=1}^{ndv} \frac{\partial f}{\partial dv_i}\,\mathrm{d}v_i \tag{16a}$$

Subject to the following:

1) Satisfaction of trim equations [balance of aerodynamic and inertial forces, Eq. (15)]

2) Hinge-moment constraints

$$HM_j^{\min} \le HM_j \le HM_j^{\max}, \qquad j = 1, \ldots, nh \tag{16b}$$

where each hinge-moment constraint is given by

$$HM_j = \sum_{i=1}^{ndv} \frac{\partial HM_j}{\partial dv_i} dv_i + HM_j^{\text{const}} \tag{16c}$$

3) Trim parameter limits (side constraints)

$$\{dv\}^{\min} \le \{dv\} \le \{dv\}^{\max} \tag{16d}$$

with design variables $\{dv\}$, where ndv is the number of trim parameters that are design variables and nh is the number of hinge-moment constraints.

The trim objective is defined as the minimization of the elastic deformations relative to some reference shape, as follows:

$$f = \sum_{n=1}^{nd} |wz_n - wz0_n| \tag{17}$$

where nd is the number of structural nodes whose displacements are to be minimized. The use of the absolute value prevents the optimization from driving the different terms $(wz_n - wz0_n)$ to large negative values.

As a result of taking the absolute value, the inherent linearity of the original objective function with respect to the design variables is eliminated. This is because the absolute value function has a discontinuous first derivative at a value of zero. Thus, the minimization of Eq. (17) does not constitute an LP problem. An equivalent LP problem can be defined with the introduction of additional nd design variables, as follows:

Minimize:

$$f = \sum_{n=1}^{nd} e_n \tag{18a}$$

Subject to the following:

1)

$$(wz_n - wz0_n) \le e_n, \qquad n = 1, \ldots, nd$$

$$-(wz_n - wz0_n) \le e_n, \qquad n = 1, \ldots, nd \tag{18b}$$

2) Satisfaction of trim equations (balance of aerodynamic and inertial forces)

3) Hinge-moment constraints [Eqs. (16b) and (16c)]

4) Trim parameter limits [side constraints, Eq. (16d)] with design variables $\{dv\}$ and $\{e\}$.

The constraints in Eq. (18b) are defined more completely as

$$-e_n - wz0_n + \sum_{i=1}^{ndv} \frac{\partial wz_n}{\partial dv_i}\,\mathrm{d}v_i + wz_{n\,\text{const}} \le 0 \tag{19a}$$

$$-e_n + wz0_n - \sum_{i=1}^{ndv} \frac{\partial wz_n}{\partial dv_i}\,\mathrm{d}v_i - wz_{n\,\text{const}} \le 0 \tag{19b}$$

where $wz_{n\,\text{const}}$ corresponds to those terms of wz_n that are not dependent on the design variables and hence remain fixed. These could include the effects of the fixed trim parameters, thickness and camber in the case of the sensorcraft, and inertial loads caused by fixed accelerations.

The design variables $\{dv\}$ for the trim optimization are trim parameters, namely, the angle of attack and deflection of the control surfaces. Six control surfaces were introduced to the sensorcraft model as shown in Fig. 3: 1) fore wing trailing-edge control surfaces (FWTE1 & FWTE2), 2) aft wing leading-edge control surfaces (AWLE1 & AWLE2), 3) outer fore wing leading-edge control surface (FWOLE), and 4) outer fore wing trailing-edge control surface (FWOTE).

The constraints selected for the trim optimization are maximum and minimum values on the hinge moments and control surface deflections. Hinge moments should not exceed some allowable values based on actuator properties. Control surface deflections should not exceed some allowable values based on control surface and actuator geometry. These allowables are defined by the user in the trim optimization scheme and are listed in Table 1 for this study.

HM_j^{const} in Eq. (16c) corresponds to those terms of the constraints that are not dependent on the design variables and hence remain fixed. These include the aerodynamic loads caused by fixed trim parameters. An example of a fixed trim parameter is the pitch rate that

Table 1 Trim-optimization constraint values

Minimum	Variable	Maximum
−5 deg	α	5 deg
−30 deg	δ_{AWLE1}	30 deg
−30 deg	δ_{AWLE2}	30 deg
−30 deg	δ_{FWOLE}	30 deg
−30 deg	δ_{FWOTE}	30 deg
−30 deg	δ_{FWTE1}	30 deg
−30 deg	δ_{FWTE2}	30 deg
−2000.0	HM_{AWLE1}, lb-ft	2000.0
−2000.0	HM_{AWLE2}, lb-ft	2000.0
−2000.0	HM_{FWOLE}, lb-ft	2000.0
−2000.0	HM_{FWOTE}, lb-ft	2000.0
−2000.0	HM_{FWTE1}, lb-ft	2000.0
−2000.0	HM_{FWTE2}, lb-ft	2000.0

is part of the trim parameter vector (as it is defined in ASTROS), but is fixed rather than designed in the trim optimization. In the sensorcraft case, the effect of thickness and camber on the aerodynamic loading is considered to be a fixed trim parameter. This has considerable effect on the hinge moments as a result of the 21% thick airfoil used. Also contributing to the constant hinge moments are the inertial loads caused by fixed accelerations.

Equations (16–19) require the sensitivities of the displacements to the trim parameter design variables ($\partial wz_n/\partial dv_i$) and the sensitivities of the hinge moments to the trim parameter design variables ($\partial HM_j/\partial dv_i$). The formulation of these sensitivities is provided in the following section.

Sensitivities with Respect to Trim Parameters Design Variables

The sensitivities of the rigid-body accelerations with respect to the ith trim parameter can be computed from Eq. (15) by assigning to $\{\delta\}$ a value of one in the ith row and zeros elsewhere. This results in the expression for the sensitivities:

$$\left\{\frac{\partial \ddot{u}_r}{\partial \delta_i}\right\} = [LHSA]^{-1}[RHSA]_i \tag{20}$$

where $[RHSA]_i = \{P_2 - K_{21}K_{11}^{-1}P_1\}_i$ is the ith column of the matrix $[RHSA]$.

The sensitivities of the r-set displacements can then be computed from Eq. (13) by again assigning $\{\delta\}$ with one in the ith row and zeros elsewhere, and by using the rigid-body accelerations of Eq. (20):

$$\left\{\frac{\partial u_r}{\partial \delta_i}\right\} = [K_{11}]^{-1}\{P_1\}_i - [K_{11}]^{-1}[K_{12}]\left\{\frac{\partial \ddot{u}_r}{\partial \delta_i}\right\} \tag{21}$$

The sensitivities of the l-set displacements can then be extracted from the first row of Eq. (10) with the same values of $\{\delta\}$, the r-set displacement sensitivities of Eq. (21), and the acceleration sensitivities of Eq. (20):

$$\left\{\frac{\partial u_l}{\partial \delta_i}\right\} = R_{11}^{-1}\{PA_l\}_i - R_{11}^{-1}R_{12}\left\{\frac{\partial u_r}{\partial \delta_i}\right\} - R_{11}^{-1}R_{13}\left\{\frac{\partial \ddot{u}_r}{\partial \delta_i}\right\} \tag{22}$$

The l-set and r-set displacement sensitivities can be merged into one vector of displacement sensitivities with respect to the ith trim parameter:

$$\left\{\frac{\partial u}{\partial \delta_i}\right\} = \left\{\begin{array}{c}\left\{\dfrac{\partial u_l}{\partial \delta_i}\right\}\\ \left\{\dfrac{\partial u_r}{\partial \delta_i}\right\}\end{array}\right\} \tag{23}$$

Substitution of $\{\partial u/\partial \delta_i\}$ into Eq. (5) provides the sensitivities of the aerodynamic forces with respect to the ith trim parameter:

$$\left\{\frac{\partial F_A}{\partial \delta_i}\right\} = q[AICS]\left\{\frac{\partial u}{\partial \delta_i}\right\} + \{PA\}_i \tag{24}$$

where $\{PA\}_i$ is the ith column of matrix $[PA]$.

Inertial loads also contribute to the component loads, and, as such, their inclusion is necessary. The inertial loads at each structural grid point $\{F_I\}$ are given by

$$\{F_I\} = \begin{bmatrix} M_{ll}D + M_{lr} \\ M_{rl}D + M_{rr}\end{bmatrix}\{\ddot{u}_r\} \tag{25}$$

and the sensitivity of the inertial loads with respect to trim parameters is given by

$$\left\{\frac{\partial F_I}{\partial \delta_i}\right\} = \begin{bmatrix} M_{ll}D + M_{lr} \\ M_{rl}D + M_{rr}\end{bmatrix}\left\{\frac{\partial \ddot{u}_r}{\partial \delta_i}\right\} \tag{26}$$

In the present study, the accelerations $\{\ddot{u}_r\}$ remain fixed. In other words, the control surfaces are deflected to trim the aircraft to a prescribed and fixed acceleration. As a result, the contribution of inertial loads to the component load constraints remains constant, and the sensitivities of Eq. (26) are disregarded.

Hinge-moment sensitivities caused by the deflection of trim parameters are calculated by multiplying the preceding aerodynamic force sensitivities, Eq. (24), by a vector that represents the moment arm from each grid point to the section about which the moment is being calculated.

Numerical Example

For this study, only a single trim condition was considered: a Mach 0.61 cruise at 65,000 ft (19.82 km) with a minimal fuel load, representing the end of the cruise before descent and landing. For this sensorcraft design, the fuel is distributed between the wings and the fuselage. This particular low fuel design point was selected for this study, as this loading case has the least inertial relief, and therefore the largest wing (and antenna) elastic deformations. Additionally, the ASTROS* (Ref. 15) code was used rather than the original ASTROS code because of the complexities associated with the aerodynamic modeling of the joined-wing layout. ASTROS* incorporates aerodynamic codes that offer greater flexibility for aerodynamic modeling of unconventional vehicles.

The trim-optimization problem just described was implemented on the sensorcraft model. Trim optimization was performed in MATLAB® using the simplex method as the optimization algorithm. As a prerequisite to the trim-optimization procedure, the sensitivities of the objective and constraints were required. These sensitivities were calculated in ASTROS* by including additional commands (reflecting the formulation detailed earlier) to the original ASTROS* MAPOL sequence. The constraints in the trim optimization were on the control surface hinge moments and deflections. The minimum and maximum values of these constraints are presented in Table 1.

Earlier, in the trim-optimization formulation section the objective function of the trim-optimization procedure was generically described as a minimization of the elastic displacements of a number of nodes on the structural model. More specifically, the trim-optimization objective was defined by the following equation:

Minimize:

$$f = |wz_{13}| + |wz_{15}| + |wz_{113}| + |wz_{115}| \tag{27}$$

Nodes 13, 15, 113, and 115 are located on the upper surface of the wing box at the 30-ft spanwise station on the fore and aft wings, corresponding to the outer edge of the X-band phased-array antenna (see Fig. 2). These nodes were selected for the objective function to represent deformations of the structure and antenna. The reference displacements $wz0_n$ of Eq. (19) were set to zero, representing the undeformed antenna position.

To provide a comparison for the results of trim optimization, six "baseline" cases were run in ASTROS*. These cases correspond to static aeroelastic analysis of the sensorcraft model in which only one control surface and the angle of attack were used to trim the aircraft in pitch and lift for a 1-g maneuver. The cases were identical, with the exception that a different control surface was used to trim the aircraft. The case number and its corresponding independent control surface are presented in Table 2.

Results and Discussion

Table 3 presents the trim parameters (control surface deflections and angle of attack) for each of the six baseline cases compared to those obtained by trim optimization (indicated by AAW). The

Table 2 Comparison baseline cases

Case No.	Independent surface
C1	AWLE1
C2	AWLE2
C3	FWOLE
C4	FWOTE
C5	FWTE1
C6	FWTE2

Table 3 Control surface deflections and angle of attack, deg

Trim parameter	C1	C2	C3	C4	C5	C6	AAW
α	−3.60	2.14	−1.85	−1.91	−3.43	−0.53	0.06
δ_{AWLE1}	NA	——	——	——	——	——	30.00
δ_{AWLE2}	——	NA	——	——	——	——	30.00
δ_{FWOLE}	——	——	−78.00	——	——	——	−30.00
δ_{FWOTE}	——	——	——	−9.26	——	——	−30.00
δ_{FWTE1}	——	——	——	——	13.97	——	−28.99
δ_{FWTE2}	——	——	——	——	——	−32.91	20.58

Table 4 Objective function vertical displacements (in feet)

Node	C3	C4	C5	C6	AAW
13	0.1260	0.1261	0.1731	0.1314	0.0125
15	−0.0103	−0.0082	−0.0061	−0.0288	0.0000
113	−0.0786	−0.0756	−0.0965	−0.1086	−0.0054
115	−0.0881	−0.0866	−0.1355	−0.1129	0.0306
rms	0.0865	0.0854	0.1195	0.1032	0.0167

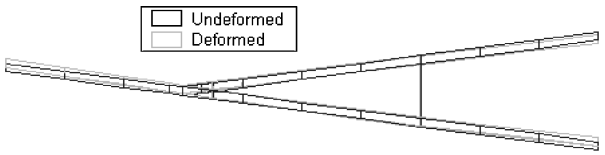

a) Case 5 (FWTE1)

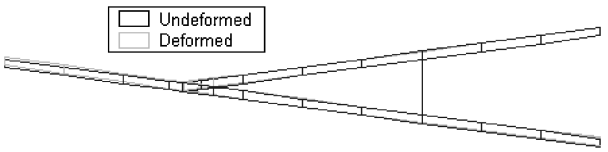

b) AAW

Fig. 4 Static aeroelastic deformation from trim solution.

trimmed negative angles of attack are the result of the built-in angles of incidence that provide positive lift at zero angle of attack. It appears from this table that the most effective surfaces for trimming the aircraft, when acting alone, are surfaces FWOTE and FWTE1, as shown by the smaller control surface deflections in cases 4 and 5. All three leading-edge surfaces seem to be impractical trim devices, as evidenced by the extremely large control surface deflections in cases 1–3 (where NA indicates that the computed deflection was larger than 90 deg). In the optimized case, however, the leading-edge surfaces are used extensively, indicating that though these surfaces might not be effective individually, they can be utilized in concert with other control surfaces to minimize the structural deformations at the antenna.

Table 4 presents the objective function displacements for the baseline cases C3–C6 and the AAW optimized case. By comparing the displacements of the optimized case to those of the other baseline cases, it is clear that the trim optimization process is effective in significantly reducing the vertical displacements of the four nodes. Cases 3–6 all exhibit quite a bit of twist in the fore wing (evidenced by the large positive displacement at node 13 and negative displacement at node 15). Although it was not part of the objective function, the optimized trim solution alleviates a significant portion of this twist. Additionally, the rms value quoted in the table is the rms of the difference between the displacements at the target nodes and the reference displacements (in this case zero). The rms values reflect the approximately order of magnitude reduction in this difference.

Figure 4 presents undeformed and deformed vehicle shapes from representative trim solutions case 5 and AAW, respectively. Although the overall size of displacements is small compared to the vehicle size, the difference between the deformed shapes can be seen from the figure. For case 5, there is a significant amount of vertical displacement in the inboard fore-wing section (the fore wing is the lower wing in this view), as well as negative displacement of the inboard section of the aft wing. Additionally, there is a significant amount of vertical deformation outboard of the joint. This outboard deformation is inconsequential to the phased-array antenna performance, as the antenna only spans the region from the centerline out to the fuselage. The optimized trim solution, Fig. 4b, reduces all of the deformations considerably, especially in the inboard region.

Table 5 Comparison of vertical displacements over the antenna structure (in feet)

Node	AAW	AAW2	AAW3	AAW4
1	−0.3297	0.0000	0.0388	0.0625
3	−0.3040	−0.0129	0.0202	0.0411
5	−0.2457	0.0012	0.0240	0.0406
7	−0.2330	−0.0302	−0.0102	0.0029
9	−0.1339	0.0237	0.0277	0.0362
11	−0.1321	−0.0260	−0.0202	−0.0150
13	0.0125	0.0816	0.0625	0.0625
15	0.0000	0.0093	−0.0019	−0.0042
101	0.3198	0.0115	0.0534	0.0516
103	0.3566	0.0123	0.0625	0.0625
105	0.2157	0.0000	0.0241	0.0186
107	0.2551	−0.0005	0.0341	0.0332
109	0.1006	−0.0159	−0.0091	−0.0153
111	0.1381	−0.0193	0.0004	0.0002
113	−0.0054	−0.0270	−0.0337	−0.0371
115	0.0306	−0.0321	−0.0234	−0.0210
rms	0.2125	0.0271	0.0335	0.0377

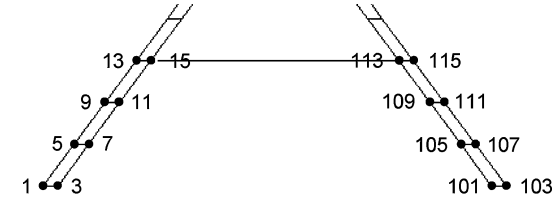

Fig. 5 Reference node locations for alternate objective function optimization.

Other Optimization Objectives

The trim-optimization objective function, as defined in Eq. (27), only addressed the vertical deflections of the four nodes corresponding to the ends of the antenna, leading to the deflections shown in Fig. 4. The deflections across the antenna are overall fairly small, but inspection of these numerical values reveals that the deflections at the objective nodes were minimized at the expense of deflections over the rest of the antenna. That is, the structural deflections inboard of nodes 13, 15, 113, and 115 are quite a bit larger than the deflections of the objective function nodes. These deflections do seem to be somewhat linear out the span, indicating that there might not be a large amount of twist and strain in these locations. This is evident in Fig. 5 and the left-hand column of Table 5, which show the locations of nodes and values of deflections at those nodes for the optimized AAW case.

As an alternative, the vertical deflections of the nodes listed in Table 5 could be included as part of the objective function, as in the following:

Minimize:

$$f = \sum |wz_n|$$

$$n \in (1, 3, 5, 7, 9, 11, 13, 15, 101, 103, 105, 107, 109, 111, 113, 115) \tag{28}$$

Trim optimization with this minimization objective leads to a new trim solution, referenced by AAW2. Table 6 presents the trim parameters, angle of attack, and control surface deflections for this trim solution as well as the original AAW solution, where it can be seen that the two objectives yield significantly different trim cases.

Table 6 Angle of attack and control surface deflections for original and alternate objective functions (in degrees)

Trim parameter	AAW	AAW2	AAW3	AAW4
α	0.06	−2.63	−1.26	−0.47
δ_{AWLE1}	30.00	30.00	30.00	0.00
δ_{AWLE2}	30.00	30.00	30.00	29.51
δ_{FWOLE}	−30.00	−18.91	−30.00	0.00
δ_{FWOTE}	−30.00	−20.08	−18.55	−23.36
δ_{FWTE1}	−28.99	−8.03	−14.46	−17.53
δ_{FWTE2}	20.58	30.00	14.10	7.53

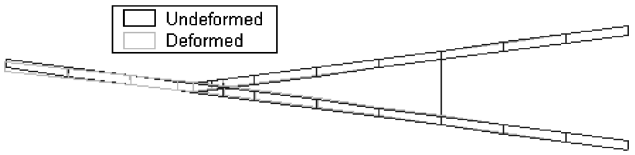

Fig. 6 Static aeroelastic deformation as a result of optimized trim solution with alternate trim objective function.

The vertical displacements of the larger set of nodes are listed in the third column of Table 5, where they can be compared to the displacements of the original AAW solution. It is clear that the AAW2 solution has larger displacements at the original four nodes, but smaller overall displacements across the antenna. The rms error of the AAW2 solution is an order of magnitude smaller than the rms error of the AAW solution as well. Figure 6 shows the deformed shape of this new solution. This solution has a slightly larger amount of twist than the original AAW solution and might in fact induce more internal strain on the embedded antenna than the original solution.

Additionally, there may also be a maximum allowable deformation value for any point on the antenna. In this case, an additional constraint on the deformations could be added to the optimization process to limit individual deformations in addition to minimizing the overall level of deformations. For instance, in the third column of Table 5, the deformation at node 13 is 0.0816 ft, just under an inch. Suppose that there was a known antenna performance constraint of 0.75 in., or 0.0625 ft. This constraint could be added to the constraint list, and the optimization process repeated. This optimization process has results in the column titled "AAW3" in Tables 5 and 6. Again, in Table 6, another completely different combination of control surface deflections is found to meet the trim balance. Note that in Table 5, each of the nodal deformations are below the limit, while the overall rms value of the deformations has increased from the AAW2 to the AAW3 solutions.

Alternatively, the optimization problem could be re-written by swapping the constraints and objective function from the AAW2 solution, resulting in an optimization problem with objective function given as the total control surface deflection, with a constraint on the deformation as in AAW3. This results in the trim solution AAW4 in Tables 5 and 6. By minimizing the control surface deflections, the trim solution finds a combination of control surfaces that satisfy the trim balance, minimize the total of the control surface deflections, and, as seen in Table 5, all have deformations below the 0.0625 ft constraint. Note that this solution has a higher rms value of deformation again as AAW3 did, but is still about an order of magnitude less than the original AAW solution.

Jig-Shape Design

Another possible solution to the antenna deformation problem is to design the vehicle with a jig shape, such that on the ground the vehicle "droops" and recovers the flat antenna shape while cruising at altitude. A simple method of determining the jig shape is to compute the deformations on the original "flat" vehicle at a trim condition, and then subtract these deformations from the undeformed shape. At that same trim condition, then, the deformed shape of the jig shape vehicle should regain the flat shape. The jig-shape method is, however, effective only for one loading case, the same loading that was used for the jig-shape design. Because the loads vary greatly during flight, in all other loading cases the antenna will be deflected. Trim optimization can then be used to minimize the antenna deformations when the loads deviate from the jig loads.

To determine the jig shape, a trim solution was computed for the midmission cruise condition, that is, with a 50% fuel load, using the FWTE1 control surface. This deformation pattern was then subtracted from the original model to obtain a jig-shape structural model, which appears in Fig. 7. The aerodynamic model was not altered. Trim solutions were obtained for 10, 50, and 90% fuel load cases using FWTE1 as the only control surface. These results are presented in Tables 7 and 8 and Fig. 8, referenced by JIG10, JIG50, and JIG90. The jig-shape design provided significant reduction of the antenna deformations (compared to the C5 column of Table 4).

Table 7 Angle of attack and control surface deflections for jig-shape solutions (in degrees)

Trim parameter	JIG10	JIG50	JIG90	JIG AAW10	JIG AAW50	JIG AAW90
α	−3.46	−2.23	−0.99	−3.66	−2.31	1.29
δ_{AWLE1}	——	——	——	−30.00	−30.00	−30.00
δ_{AWLE2}	——	——	——	−28.47	−18.76	30.00
δ_{FWOLE}	——	——	——	30.00	30.00	−11.16
δ_{FWOTE}	——	——	——	3.31	−18.25	−30.00
δ_{FWTE1}	11.63	26.05	40.44	19.04	18.45	9.80
δ_{FWTE2}	——	——	——	−8.23	30.00	30.00

Table 8 Displacement error (from flat shape) for jig-shape solutions (in feet)

Node	JIG10	JIG50	JIG90	JIG AAW10	JIG AAW50	JIG AAW90
13	−0.0439	0.0153	0.0716	−0.0005	−0.0068	−0.0239
15	0.0092	−0.0180	−0.0443	0.0024	−0.0004	−0.0204
113	0.0327	−0.0394	−0.1086	0.0045	0.0029	−0.0180
115	0.0465	−0.0547	−0.1545	0.0047	0.0047	0.0047
rms	0.0362	0.0357	0.1034	0.0035	0.0044	0.0182

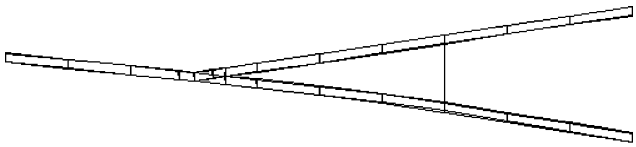

Fig. 7 Undeformed jig shape based on 50% fuel load and FWTE1.

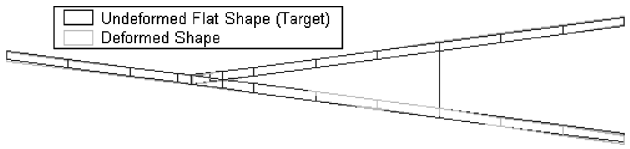

a) JIG10

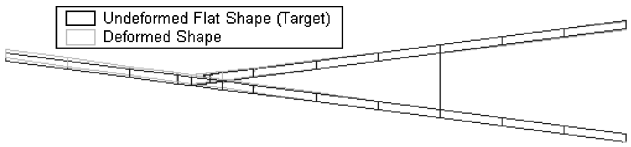

b) JIG50

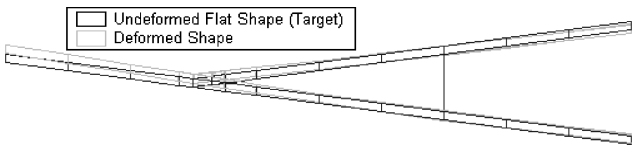

c) JIG90

Fig. 8 Static aeroelastic deformation of jig-shape trim using FWTE1 compared to undeformed flat shape.

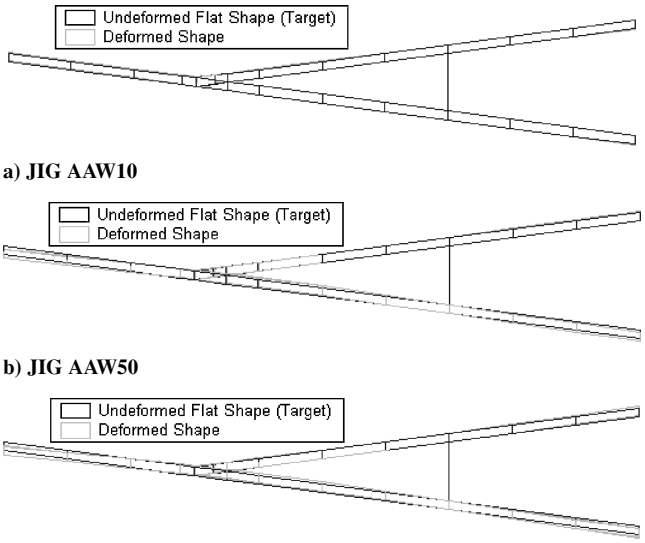

Fig. 9 Static aeroelastic deformation of jig-shape trim optimization compared to undeformed flat shape.

However, in the off-design case of 90% fuel the deflections were relatively large, and demonstrate the fact that a jig-shape approach by itself is not enough to reduce deformations to an acceptable level.

Trim optimization was then applied to the jig-shape model, and solutions were obtained for the three loading cases. For these cases, the reference displacements $wz0_n$ of Eq. (19) were no longer zero, but were the original displacements used to define the jig shape. The results of these computations are also shown in Tables 7 and 8 and Fig. 9, referred to as JIGAAW10, −50, and −90. With trim optimization, all three loading cases are quite adequately handled, even the two off-design points. The 10 and 50% fuel cases have excellent results, and their rms errors are several times smaller than the original AAW solution. In the 90% fuel case, trim optimization reduced the deflections by and order of magnitude, to the same rms level as in the original AAW solution.

Maneuver

One issue that is often mentioned when discussing the cruise trim analysis is the control surface constraints in the optimization process. In the examples above, a limit of ±30 deg is used. Many consider this to be too large a constraint, as it doesn't allow any "excess" control surface for maneuvering off of the cruise condition. Hopefully, by now it has been demonstrated sufficiently that one can find an optimized trim condition for any maneuver in the same manner as determining the initial cruise trim, rather than maneuvering by perturbing the control surface settings from the cruise trim. This maneuver trim will have a completely different combination of control surface settings, such that no excess control surface is required from the cruise solution.

As an example, the optimization process was repeated with a roll analysis to demonstrate the maneuver trim optimization and its effects on the deformation. This example starts from the 10% fuel condition at the end of cruise, and we assume that the aircraft is trimmed in cruise with the control surface settings determined by the optimization AAW2 (Table 6). The roll rate goal is approximately 13 deg/s,[16] which represents a first-order approximation of the roll rate required for the sensorcraft to reach 30 deg in 2–3 s.

From this initial cruise trim setting AAW2, several different roll trim solutions are determined. The first is determined by finding the control surface with the largest effectiveness in roll based on the rolling moment coefficient (FWOTE), and deflecting only that control surface until the aircraft is trimmed in roll. This solution appears in the first column in Table 9 as trim solution ΔAAW2. Note that as a perturbation from cruise trim AAW2 (Table 6), the deflection of FWOTE has gone from –20.08 to –12.76 deg. This is a perfectly acceptable trim solution, but it is not the only solution. Unfortunately, the vehicle is extremely flexible, and the rolling motion of the vehicle causes a very large level of antenna deformations, such that it would be impossible to continue antenna operation during roll. Therefore, the objective function of minimum antenna deformation, while still valid, is not plausible in this case. However, other objective functions can be used, related to minimizations of total hinge moment, actuator work required to deflect the control surface, or aerodynamic energy required to deflect the control surface,[16] all using an equality trim constraint based on a roll trim balance. These objective functions: total hinge moment, actuator work, and aerodynamic energy, are all implemented in Matlab and used to solve the roll trim optimization problem. Solutions to these, labeled AAWR1-AAWR3 in Table 9, demonstrate several different combinations of control surfaces capable of trimming the vehicle. The three solutions show that, depending on the vehicle and maneuver requirements, it may not be necessary to hold excess control surface "in reserve" when considering deformation limits or other optimization objectives.

Table 9 Control surface effectiveness and deflections (in degrees) for a roll trim case

Trim Parameter	ΔAAW2 (FWOTE)	AAWR1	AAWR2	AAWR3
δ_{AWLE1}	30.00	−30.00	1.00	0.04
δ_{AWLE2}	30.00	−30.00	0.57	0.12
δ_{FWOLE}	−18.91	30.00	−0.51	0.12
δ_{FWOTE}	−12.76	−23.80	−0.17	1.09
δ_{FWTE1}	−8.03	30.00	23.62	30.00
δ_{FWTE2}	30.00	30.00	5.42	1.52

Conclusions

The active-aeroelastic-wing program has demonstrated maneuver performance benefits from multiple control surfaces. This study has conceptually demonstrated other benefits that are achievable through this same concept, in particular the reduction of antenna deformations in a joined-wing sensorcraft configuration, for antenna performance improvements.

Trim optimization was performed, in which the deflections of six control surfaces were optimized to minimize the antenna deformations, simultaneously trimming the aircraft to the required 1-g level flight and maintaining constraints on the allowable hinge moments and maximum control surface deflections. With the optimal control surface deflections, antenna deformations were reduced by an order of magnitude compared to a traditional trim solution that makes use of one control surface only (traditional trim). Two variants of the objective function were studied, leading to different trim solution and deflected antenna shape.

Trim optimization was also combined with a jig-shape design approach, in an attempt to further reduce the antenna deformations. This resulted in excellent, very low deformations under some loading cases, whereas in another loading case the deformations were of the same order of magnitude as the original trim optimization (one order-of-magnitude reduction compared to the traditional trim).

Finally, a roll trim optimization was conducted to illustrate the possibility of maneuvering while simultaneously maintaining low deformation levels. This also addresses the issue of control surface deflection limits, and demonstrates that keeping excess control surface deflection in reserve may not be necessary.

This study joins the referenced literature on active aeroelastic wing, showing that the concept holds promise for various aeroelastic shape control applications, as well as providing a basis for more radical aircraft morphing concepts.

References

[1] Volk, J. A., and Ausman, J. D., "Integration of a Generic Flight Control System into ASTROS," AIAA Paper 96-1335, April 1996.

[2] Ausman, J. D., and Volk, J. A., "Integration of Control Surface Load Limiting into ASTROS," AIAA Paper 97-1115, April 1997.

[3]Miller, G. D., "An Active Flexible Wing Multi-Disciplinary Design Optimization Method," AIAA Paper 94-4412-CP, Sept. 1994.

[4]Zillmer, S., "Integrated Multidisciplinary Optimization for Active Aeroelastic Wing Design," Air Force Wright Aeronautical Labs., WL-TR-97-3087, Dayton, OH, Aug. 1997.

[5]Love, M. H., Barker, D. K., Egle, D. D., Neill, D. J., and Kolonay, R. M., "Enhanced Maneuver Airloads Simulation for the Automated Structural Optimization System—ASTROS," AIAA Paper 97-1116, April 1997.

[6]Zink, P. S., Mavris, D. N., and Raveh, D. E., "Maneuver Trim Optimization Techniques for Active Aeroelastic Wings," *Journal of Aircraft*, Vol. 38, No. 6, 2001, pp. 1139–1146.

[7]"ZAERO Version 4.0 Theoretical Manual," 7th ed. 99–11, ZONA Technology, Inc., Scottsdale, AZ, Nov. 1999.

[8]Bowman, J. C., Sanders, B., and Weisshaar, T., "Identification of Military Morphing Aircraft Missions and Morphing Performance Assessment," *Society of Photo-Optical Instrumentation Engineers Conference on Industrial and Commercial Applications of Smart Structures Technologies*, edited by A. R. McGowan, Vol. 4698, SPIE, Bellingham, WA, 2002, pp. 121–132.

[9]Wlezien, R. W., Horner, G. C., McGowan, A. R., Padula, S. L., Scott, M. A., Silcox, R. J., and Simpson, J. O., "The Aircraft Morphing Program," *Society of Photo-Optical Instrumentation Engineers Conference on Industrial and Commercial Applications of Smart Structures Technologies*, edited by J. M. Sater, Vol. 3326, SPIE, Bellingham, WA, 1998, pp. 176–187.

[10]DARPA, BAA 01-42, Addendum 7, Special Focus Area: Morphing Aircraft Structures (MAS), Dec. 2001.

[11]Johnson, E. H., and Venkayya, V. B., "ASTROS Theoretical Manual," AFWAL-TR-88-3028, December 1988.

[12]Mrozinski, D. P., Zeh, J. M., Reich, G. W., Carter, D. L., Cord, T. J., and Shenk, B., "Simulation-Based Research and Development Technology Assessment Process," *Society of Photo-Optical Instrumentation Engineers Conference on Enabling Technology for Simulation Science VI*, edited by A. F. Sisti and D. A. Trevisani, Vol. 4716, SPIE, Bellingham, WA, 2002, pp. 286–294.

[13]"Jane's Unmanned Aerial Vehicles and Targets," Jane's Information Group. Coulsdon, Surrey, UK, 2003.

[14]Chvátal, V., *Linear Programming*, W. H. Freeman and Co., New York, 1983, p. 222.

[15]Chen, P. C., Sarhaddi, D., and Liu, D. D., "Development of the Aerodynamic/Aeroservoelastic Models in ASTROS, Vol. 4: ZAERO Theoretical Manual," U.S. Air Force Research Lab., AFRL-VA-WP-TR-1999-3052, edited by E. J. Breitback, L. F. Campanile, and H. P. Monner, CRC Press, New York, Feb. 1999.

[16]Reich, G. W., Bowman, J. C., and Sanders, B., "Application of Adaptive Structures Technology to High Altitude Long Endurance Sensor Platforms," *13th International Conference on Adaptive Structures and Technologies*, Potsdam, Germany, Oct. 2002.